

# Diffusion Model Driven Airfoil Design: From Geometry Encoding to Practical Applications

Yingfan Geng <sup>\*</sup>, Jinhong Wang <sup>†‡</sup>, and Teng Cao <sup>§¶</sup>

*Imperial College London, South Kensington, Greater London Area, United Kingdom, SW7 2AZ*

**Diffusion model, the state-of-the-art generative machine learning architecture, has shown promising results airfoil inverse designs. In this study, we implemented and trained a series of diffusion models on three different airfoil geometry data encoding formats – principal component weights, ordered  $x$ - $y$  coordinates, and 2D signed distance functions (SDF) – to generate 2D airfoils. By systematically comparing the performance of diffusion models trained on different data structures, it is found that for 2D airfoil design problems, the diffusion model performs the best when directly trained with coordinates. Training with latent space (PCA weights in this study) limits the model’s design freedom, and decreases the training effectiveness. Although the 2D SDF data appears to result in the least performing model, it proves its feasibility in aerodynamic shape generation, paving the way towards 3D problems where SDF is more favored. This study also investigated deploying the diffusion model in practical engineering applications. A multi-target optimization procedure is proposed based on the stochastic nature of the diffusion process, which drastically simplifies the procedure compared to conventional methods. The extrapolation performance of the model is also investigated by tasking the model with both aerodynamic and flow condition labels that are extrapolated beyond the training set boundaries.**

---

<sup>\*</sup>Research Student, Department of Mechanical Engineering.

<sup>†</sup>Research Associate, Department of Mechanical Engineering.

<sup>‡</sup>Equal first author.

<sup>§</sup>Assistant Professor, Department of Mechanical Engineering.

<sup>¶</sup>Corresponding Author: t.cao@imperial.ac.uk

## Nomenclature

### *Roman letters*

$C_L$	=	lift coefficient
$C_D$	=	drag coefficient
$C_M$	=	pitch moment coefficient
$C_P$	=	pressure coefficient
$D$	=	neural network
$Ma$	=	Mach number
$Re$	=	Reynolds number
$\mathbf{x}$	=	data

### *Abbreviations*

AOA	=	angle of attack
CFD	=	computational fluid dynamics
CST	=	class-shape transformation
DDPM	=	denoising diffusion probabilistic model
EDM	=	elucidating diffusion model
GAN	=	generative adversarial network
PCA	=	principal component analysis
RMSE	=	root-mean-square error
SDF	=	signed distance function
UIUC	=	University of Illinois Urbana-Champaign
VAE	=	variational auto-encoder

### *Greek letters*

$\varepsilon$	=	tolerance
$\sigma$	=	noise level

## I. Introduction

Aerodynamic optimization plays a critical role across aerospace applications, with airfoil design as a central example because it determines the aerodynamic efficiency and, ultimately, the economic performance of an aircraft. Airfoil design, which is essentially finding a geometry that meets specified performance targets under given operating conditions, is a challenging inverse problem due to non-linear flow physics, multi-objective trade-offs, and strict geometric and operational constraints.

Traditional airfoil design workflows follow iterative loops together with geometry parameterizations. Initial design begins with a selection of parametrization (e.g., NACA families or class-shape transformation (CST) function [1]), and empirically derived guidelines are followed. The initial design concepts were then validated with computational fluid dynamics (CFD) or wind-tunnel testing for more accurate performance metrics [2]. The geometry parameters are then optimized until all requirements are met. While the geometry parametrization reduces the computational costs, it also limits the admissible design space and can lead to suboptimal outcomes. This motivates the development of high-dimensional inverse-design methods for broader, more efficient exploration without the constraints induced by geometry parametrization. A typical example of this is the free-form deformation optimization [3], where the 3D geometry mesh is directly optimized using the adjoint gradient method.

With the significant development of machine learning in recent years, both machine learning based forward surrogate and inverse design models have emerged. Forward surrogate models [4] use trained neural networks as a replacement for physical simulation tools (e.g., Xfoil [5]) to reduce the computational resources required during design iterations. Direct inverse design models, which originate from image synthesis tasks, can directly generate the airfoil geometry given a set of condition inputs. The two most popular generative architectures are the variational auto-encoder (VAE) [6] and generative adversarial network (GAN) [7]. Furthermore, Lei *et al.* [8] also used the CLIP architecture to achieve airfoil generation with natural language as inputs. Compared to traditional methods, generative models greatly expand the design space and simplify the optimization procedure. More recently, the diffusion probabilistic model [9], which was inspired by non-equilibrium thermodynamics, demonstrated superior performance over VAE and GAN on a broad range of image-generation benchmarks [10], and are widely regarded as the state-of-the-art generative method. Having proven effective for complex image synthesis, diffusion models offer the controllability and reliability required to tackle engineering problems under stringent physical constraints, making them potential candidates for inverse design problems. The stochastic nature of the diffusion model aligns naturally with the one-to-many mapping characteristic of inverse design problems: multiple distinct geometries can satisfy the same target performance metric. Unlike deterministic inverse design methods, which produce a single solution, the diffusion-based approach inherently generates diverse designs that meet the specified targets. While promising, its application to engineering design problems – and, specifically, to airfoil generation – is still in an early research stage.

A common strategy in the literature is to train diffusion models in a latent space to reduce data dimensionality

and promote smoothness of the generated shapes. Diniz *et al.* [11] proposed a conditional diffusion framework that optimizes airfoil geometry under specified flow and aerodynamic conditions, conditioning on Mach number ( $Ma$ ), Reynolds number ( $Re$ ), and lift coefficient ( $C_L$ ). Their approach first encodes geometry via a learned Variational Auto-Encoder (VAE), then samples airfoils with diffusion to satisfy target conditions; the objective is to minimize the drag coefficient ( $C_D$ ) subject to geometric constraints. Wei *et al.* [12] followed a similar latent-space paradigm and compared diffusion with traditional GAN baselines, reporting advantages for diffusion in airfoil generation fidelity and controllability. Beyond learned latent spaces, several works parameterize the airfoil explicitly via classical curve families or statistical bases: Wen *et al.* [13] employed class-shape transformation (CST) and Bézier curves, while Zhuang *et al.* [14] used principal component analysis (PCA) to represent geometry via principal component coefficients. Deng *et al.* [15] further explored conditioning via an intermediate physical representation by diffusing the pressure-coefficient curve  $C_P$  (with a 7-parameter characterization), followed by a learned mapping from  $C_P$  to the corresponding airfoil shape; this retains more aerodynamic structure than generic latent spaces. While latent-space diffusion simplifies training and enforces smoothness [16], it is effectively equivalent to geometry parameterization that was used in the traditional methods as discussed previously, and hence will constrain the admissible design space and limit the exploration of novel, unconventional airfoil configurations. In contrast, direct diffusion on explicit geometry representations offers greater design freedom but poses additional modeling and stability challenges. In generic 2D/3D shape generation, researchers have explored multiple explicit formats, including point sets, point clouds [17], voxel grids [18], and signed distance fields (SDFs) [19]. Within airfoil generation tasks, direct coordinate diffusion (i.e., ordered contour coordinates) has seen limited trials and mixed results [20], and there is a lack of systematic comparisons across multiple geometry encodings (latent vs. explicit) under a common diffusion backbone.

Methodologically, most airfoil studies to date adopt the original denoising diffusion probabilistic model (DDPM) [9]. However, the elucidated diffusion framework (EDM) [21], which employs continuous noise characterization and high-order ODE-based samplers, has been shown to reduce sampling steps and improve stability in image synthesis tasks. Its potential advantages for engineering inverse design, especially under multi-condition constraints and explicit geometry encodings, remain under-explored.

In addition, condition labels in the literature can be grouped into three categories: (i) *flow conditions* (e.g.  $Re$ ,  $Ma$ , angle of attack  $AOA$ ), (ii) *aerodynamic targets* (e.g.  $C_L$ ,  $C_D$ ,  $C_M$ ), and (iii) *geometric constraints* (e.g. maximum thickness, leading-edge radius, trailing-edge angle). Most studies employ single-condition labeling or narrow multi-condition ranges [12, 13, 15, 20, 22], with few works demonstrating multi-condition labeling across  $Re$ ,  $Ma$ , and  $AOA$  [11, 14, 23].

The current literature reveals three key gaps. First, there is no systematic evaluation of diffusion performance across diverse geometry encoding methods (e.g., PCA latent space, ordered coordinates, SDF grids) within a unified framework. Second, conditioning across broad ranges of  $AOA$ ,  $Re$ , and  $Ma$  is limited with most studies rely on single-

condition labels or narrow multi-condition spans. Third, state-of-the-art diffusion samplers like EDM have not been systematically examined for airfoil inverse design, despite their efficiency and stability benefits. Addressing these gaps can clarify trade-offs among representations, improve robustness across operating conditions, and accelerate practical adoption in engineering design workflows.

To address these gaps, we present a unified, conditional diffusion model based generative framework for two-dimensional airfoil inverse design. In this study, three geometry encoding methodologies are systematically evaluated – principal component weights (PCA), ordered coordinates, and 2D signed distance function (SDF) – within an elucidated diffusion model (EDM) backbone. The model jointly conditions on angle of attack  $AOA$ , Reynolds number  $Re$ , and Mach number  $Ma$  across broad ranges, demonstrating strong accuracy, robust constraint satisfaction, and deployment-ready workflows. By consolidating insights in 2D generation under realistic operating constraints, this work establishes a principled foundation for extending diffusion-based design to complex three-dimensional aerodynamic geometries.

## II. Methodology

In this section, the workflow of the diffusion model implementation and development is introduced, as illustrated in Fig. 1.

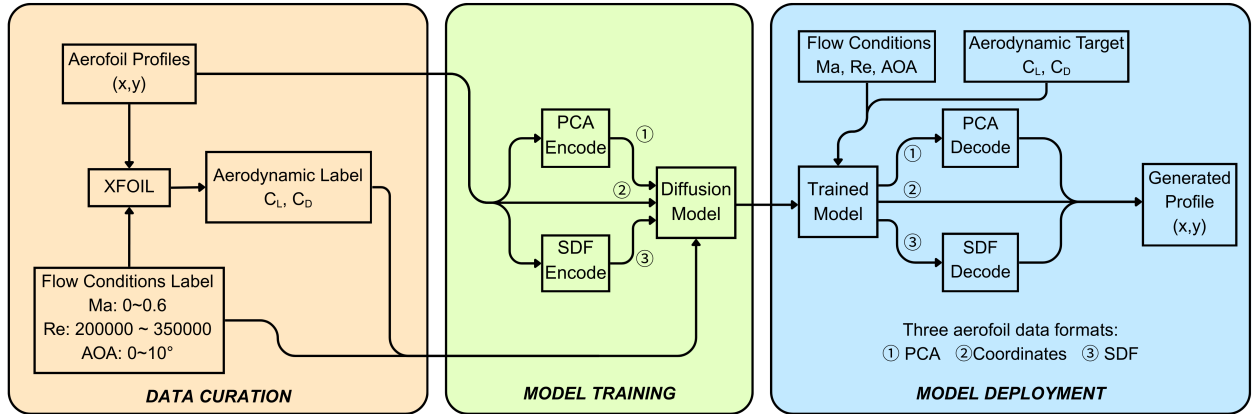


**Fig. 1 Workflow of Diffusion Model Training and Deployment**

### A. Data curation and Preprocessing

#### 1. Airfoil Database and Label Generation

Airfoil geometries that were used in this study are from the UIUC airfoil database [24]. This database contains  $\sim 1500$  airfoil profiles from various design families such as the NACA and Eppler series, for various applications. After excluding the designs with non-closed trailing edge, there are in total 1474 profiles to form the model's training dataset. The airfoil chord is non-dimensionalized such that the leading and trailing edges are located at  $(0, 0)$  and  $(1, 0)$ , respectively. The distribution of the airfoil profiles are illustrated as kernel density estimates (KDE) plot, shown

in Fig. 2a for reference.

XFOIL, a 2D airfoil analysis tool using the panel method, is used as the surrogate simulation model to create the aerodynamic labels [5]. XFOIL's interpolation tool is also used to smooth the profile shape and ensure an equal number of coordinate points for each profile. In this study, 256 points per profile are maintained. Flow conditions are sampled on a uniform grid: Reynolds number ( $Re$ ) from  $2 \times 10^5$  to  $3.5 \times 10^5$  in increments of  $5 \times 10^4$ ; Mach number ( $Ma$ ) from 0 to 0.6 in increments of 0.1; and angle of attack ( $AOA$ ) from  $0^\circ$  to  $10^\circ$  in steps of  $1^\circ$ . All endpoints are inclusive.

The corresponding  $C_L$  and  $C_D$  for different airfoils are then calculated using XFOIL with their distribution shown in Fig. 2b. The specified flow conditions ( $Ma$ ,  $Re$ , and  $AOA$ ) and the aerodynamic performance ( $C_L$  and  $C_D$ ) form the condition label of the diffusion model. For flow-condition combinations under which an airfoil is unlikely to operate properly (e.g., post-stall at high  $AOA$ ), XFOIL may fail to converge and return no solution. These cases are flagged as non-convergent and excluded from the dataset. To reduce the impact of outliers, samples outside the range of  $C_L \in [0, 2.0]$  or  $C_D \in [0, 0.05]$  are excluded (endpoints inclusive). The final dataset contains 372,924 data entries.

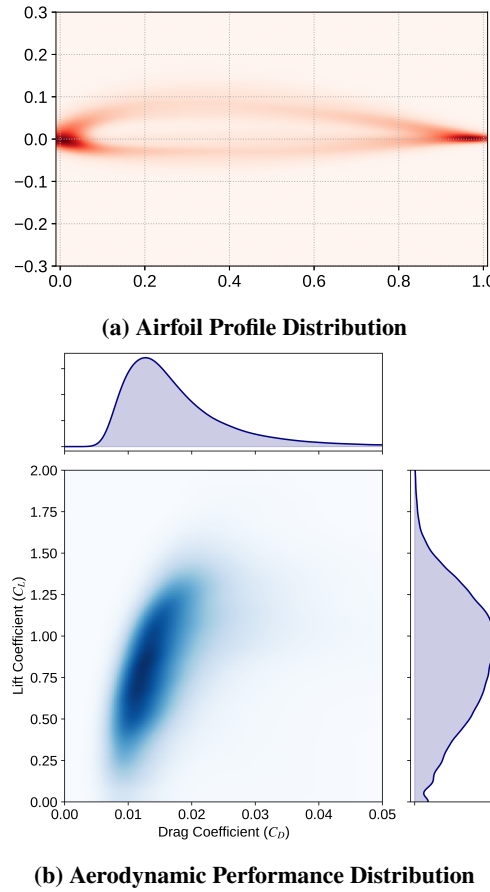


**Fig. 2 The Diffusion Model Dataset Distribution**

## 2. Geometry Representation

As introduced in Section I, the previous studies in literature have all parametrized the airfoils into latent space before training the diffusion model. Although by doing so reduces the data dimensionality as well as the training complexity, it also limits the model's design freedom. Therefore, in this study, we present three different airfoil geometry representation approaches: (i) principal component analysis (PCA); (ii) ordered  $x$ - $y$  coordinates; and (iii) signed distance function (SDF), as shown in Fig. 3.

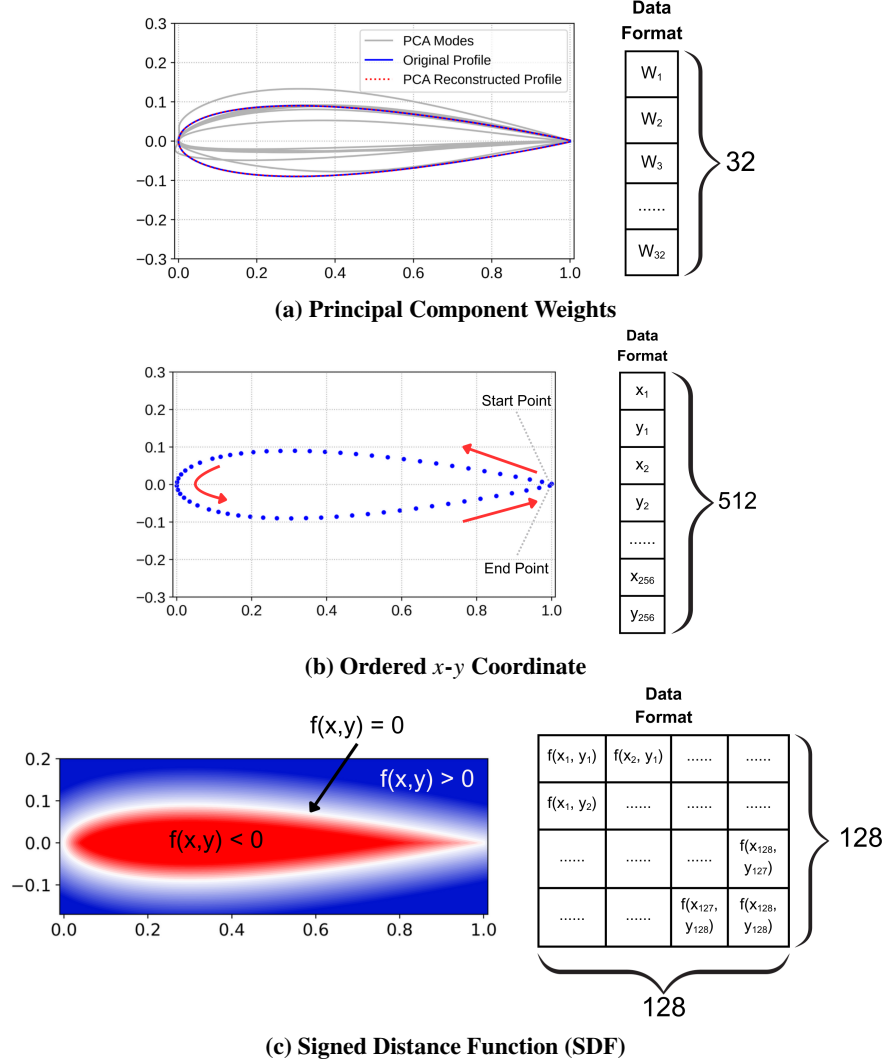


**Fig. 3** Different data structures to encode the airfoil geometry.

**Principal Component Weights** Principal component analysis (PCA) is a statistical tool that maps a complex dataset to a lower dimension [25]. PCA identifies the principal axes along which the data exhibit the largest variance, corresponding to the dominant modes of the dataset. In this present study, by conducting PCA, the data is reaped from  $\mathbf{X} \in \mathbb{R}^{256}$  to  $\mathbf{X} \in \mathbb{R}^N$  where  $N$  is the number of principal components (PC). Increasing  $N$  improves the accuracy of the

PCA representation of the airfoil data, which is characterized by the explained variance ratio, defined as Eq. (1),

$$\text{Explained Variance Ratio} = \frac{\sum_{i=1}^N \lambda_i}{\sum_{j=1}^{256} \lambda_j} \quad (1)$$

where  $\lambda$  is the eigenvalue of the covariance matrix of the corresponding PC. The accuracy of PCA with different  $N$  is shown in Fig. 4. In this study,  $N = 32$  is chosen, which corresponds to 99.99 % of accuracy to ensure that there is only negligible amount of information loss during the PCA process. As a result, the PCA-based data encoding produces an array of 32 real numbers, as shown in Fig. 3a, each of representing the weight of the corresponding principal component (shown as gray curves). The original profile (blue curve) can then be reconstructed by a linear combination of these 32 principal components using the corresponding principal component weights (reconstructed profile shown as red curves). The PCA are fitted after coordinates normalization for consistency.

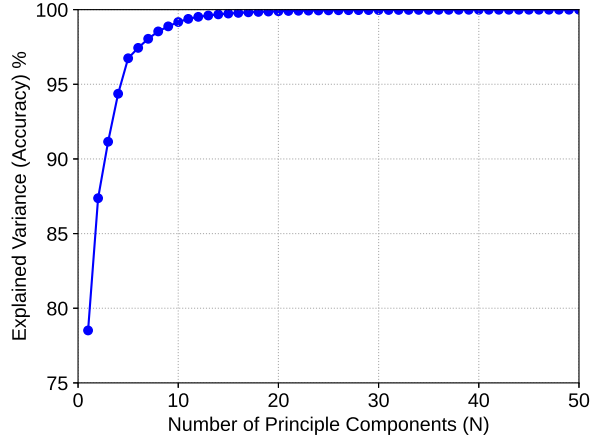


**Fig. 4 PCA Accuracy**

**Ordered coordinate** The second approach takes data directly from the dataset with no additional encoding. The coordinates are arranged in a specific order: counter-clockwise starting from the trailing edge to the leading edge, and returning to the trailing edge, as illustrated in Fig. 3b. This is consistent with the default arrangement from the UIUC database [24], and matches required profile data format by XFOIL [5]. This also enhances the spatial information, which benefits the subsequent training of the diffusion model.

**Signed distance function (SDF)** Signed distance function (SDF), also referred to as a signed distance field, is a continuous function that describes the shortest distance from any point to the object boundary. Points inside the object have negative SDF values while points outside have positive values. The points on the object edge have SDF values of 0. Previous studies in the field of generic object generation has shown the advantages of using SDF compared to other data formats [19].

In this study, the SDF matrix is defined with a size of  $128 \times 128$ , as shown in Fig. 3c. The SDF values  $f(x, y)$  are normalized to  $[-1, 1]$  to retain the sign information during training. During the SDF decoding process, the zero-valued contour points are extracted. To ensure profile smoothness, quadratic interpolation is applied, and the recovered geometry points are reordered in the manner as in Fig. 3b for XFOIL compatibility.

### 3. Data Summary

To ensure equal contribution of all features to model, all condition labels ( $Ma$ ,  $Re$ ,  $AOA$ ,  $C_L$ , and  $C_D$ ) are normalized to a range of  $0 \sim 1$  using min-max normalization. The dataset is then split into training, validation, and testing sets with an 8:1:1 ratio. The same dataset was used for all three data structures for comparison.

## B. Diffusion Framework

A conditional diffusion model is used as the backbone in this study. Conceptually, the model is a denoising predictor, that receives a noisy geometry signal together with a conditioning vector (operating/design labels) and a noise level, and returns a prediction of the corresponding clean signal. The core denoising functionality is implemented via a neural network, denoted here by  $D$ , which will be introduced in Section II.C.

The mathematical formulation of the diffusion model used in this study follows the Elucidating Diffusion Model (EDM) framework introduced by Karras *et al.* [21], which is a variant from the original DDPM model [9] with improved performance. The fundamental diffusion process is governed by the probability flow ODE and the stochastic diffusion equation (SDE), as shown in Eq. (2) [26].

$$d\mathbf{x}_\pm = \underbrace{-\dot{\sigma}(t)\sigma(t)\nabla_{\mathbf{x}} \log p_t(\mathbf{x}; \sigma(t))dt}_{\text{probability flow ODE}} \pm \underbrace{\beta(t)\sigma(t)^2\nabla_{\mathbf{x}} \log p_t(\mathbf{x}; \sigma(t))dt + \sqrt{2\beta(t)}\sigma(t)d\omega_t}_{\text{Langevin diffusion SDE}} \quad (2)$$

The first term (deterministic probability flow ODE) guides the diffusion trajectory towards the region of higher likelihood for the clean data. The second part of Eq. (2) is the Langevin SDE, which introduces stochasticity to the diffusion process to increase the diversity of generated outputs and is emulated by using a temporary addition of Gaussian noise.

In Eq. (2),  $t \in [0, T]$  denotes a continuous time variable of the diffusion process,  $\mathbf{x}$  is the data,  $p_{\mathbf{x}}$  is the probability distribution of the data, and  $\sigma$  is the standard deviation of the signal as a representation of the noise level. The score function  $\nabla_{\mathbf{x}} \log p_t(\mathbf{x}; \sigma(t))$  is defined as Eq. (3) [26] and it points towards the higher data density region at a given noise level of  $\sigma(t)$ .

$$\nabla_{\mathbf{x}} \log p_t(\mathbf{x}; \sigma(t)) = \frac{D(\mathbf{x}; \sigma) - \mathbf{x}}{\sigma^2} \quad (3)$$

The training objective follows the Elucidating Diffusion Model (EDM) formulation [21] and minimizes the expected weighted mean-squared error between the network output and the ground truth. The weighting function  $\lambda(\sigma)$  and the

scaling coefficients  $c_{\text{in}}(\sigma)$ ,  $c_{\text{out}}(\sigma)$ ,  $c_{\text{skip}}(\sigma)$ , and  $c_{\text{noise}}(\sigma)$  are noise-dependent hyper-parameters defined according to the EDM framework. The overall objective is to minimize the expected loss given in Eq. (4).

$$\mathbb{E}_{\sigma, x, n} \left[ \underbrace{\lambda(\sigma) c_{\text{out}}^2}_{\text{weight}} \underbrace{\| F_{\theta}(c_{\text{in}}(\sigma) \cdot (x + n); c_{\text{noise}}(\sigma)) - \underbrace{\frac{1}{c_{\text{out}}(\sigma)} (x - c_{\text{skip}}(\sigma) \cdot (x + n)) \|_2^2}_{\text{ground truth}} }_{\text{neural network output}} \right] \quad (4)$$

After training, the denoising process is explained in Algo. 1. The initial signal  $\mathbf{x}_0$  is sampled from a pure Gaussian noise, and the diffusion model is applied to progressively denoise the signal until a clean sample  $\mathbf{x}$  is obtained. The noise level scheduled along the denoising trajectory is scheduled by  $\left( \sigma_{\text{max}}^{\frac{1}{\rho}} + \frac{i}{N-1} \left( \sigma_{\text{min}}^{\frac{1}{\rho}} - \sigma_{\text{max}}^{\frac{1}{\rho}} \right) \right)^{\rho}$ , where  $N$  is the total number of denoising steps,  $i$  denotes the current denoising step and  $\rho$  is a tunable hyper-parameter. It is noted that during the sampling procedures, there is an additional step of temporary noise addition (line 6 in Algo. 1), which adds additional stochasticity to achieve greater diversity in generated designs. In addition, compared to the original DDPM sampling process [9], the EDM architecture samples the noise with a second order approach (line 9 – 12 in Algo. 1), which reduces the amount of intermediate steps required during design generation. In this study, all hyper-parameters settings are kept as default as in [21].

---

**Algorithm 1** Diffusion model generation

---

```

1: procedure Stochastic Sampler ( $D(\mathbf{x}; \sigma)$ ,  $t_i \in \{0, \dots, N\}$ ,  $\gamma_i \in \{0, \dots, N-1\}$ ,  $S_{\text{noise}}$ )
2: sample  $\mathbf{x}_0 \sim \mathcal{N}(\mathbf{0}, t_0^2 \mathbf{I})$ 
3: for  $i \in \{0, \dots, N-1\}$  do
4:   sample  $\epsilon_0 \sim \mathcal{N}(\mathbf{0}, S_{\text{noise}}^2 \mathbf{I})$ 
5:    $\gamma_i = \begin{cases} \min\left(\frac{S_{\text{churn}}}{N}, \sqrt{2} - 1\right) & \text{if } t_i \in [S_{\text{tmin}}, S_{\text{tmax}}] \\ 0 & \text{otherwise} \end{cases}$ 
6:    $\hat{t}_i \leftarrow t_i + \gamma_i t_i$  ▷ add noise temporarily to emulate the stochastic diffusion
7:    $\hat{\mathbf{x}}_i \leftarrow \mathbf{x} + \sqrt{\hat{t}_i^2 - t_i^2} \epsilon_i$ 
8:    $\mathbf{d}_i \leftarrow (\hat{\mathbf{x}}_i - D(\hat{\mathbf{x}}_i; \hat{t}_i)) / \hat{t}_i$ 
9:    $\mathbf{x}_{i+1} \leftarrow \hat{\mathbf{x}}_i + (t_{i+1} - \hat{t}_i) \mathbf{d}_i$  ▷ linear Euler step for solving probabilistic flow ODE
10:  if  $t_{i+1} \neq 0$  then
11:     $\mathbf{d}'_i \leftarrow (\mathbf{x}_{i+1} - D(\mathbf{x}_{i+1}; t_{i+1})) / t_{i+1}$  ▷ Huen method correction
12:     $\mathbf{x}_{i+1} \leftarrow \hat{\mathbf{x}}_i + \frac{1}{2}(t_{i+1} - \hat{t}_i)(\mathbf{d}_i + \mathbf{d}'_i)$ 
13:  end if
14: end for

```

---

### C. Model Architecture

As introduced in Section II.B, a neural network  $D$  is trained as the core of the denoising process. In this present study, U-Net [27] is implemented as the noise predictor. Due to its symmetric architecture with the same input and output dimensions, U-Net is the most commonly adopted network architecture in diffusion models [9, 13, 28]. In addition, following standard practice in deep learning, residual networks (ResNet [29]) are adopted as the basic convolutional

building blocks. The overall architecture is illustrated in Fig. 5.

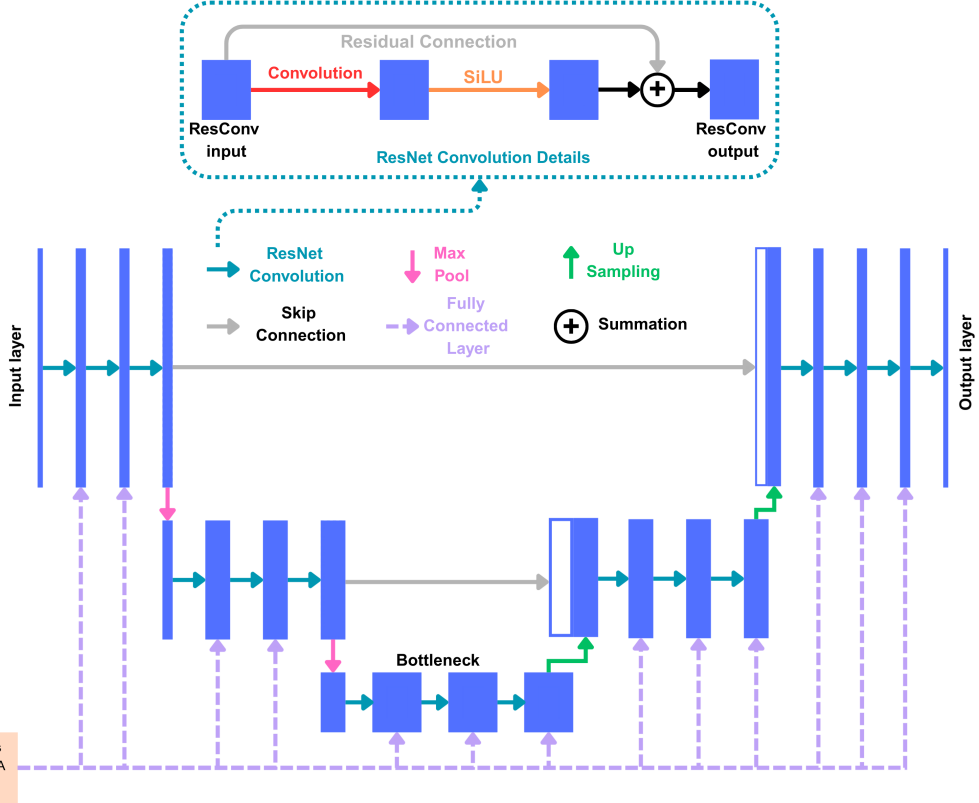


**Fig. 5 Neural Network Architecture: U-Net with ResNet blocks**

The basic network architecture is identical for the three input data formats introduced in Section II.A.2, with the only difference being the number of ResNet blocks used per layer of the U-net (i.e., number of blocks on each downsampling stages in Fig. 5). The U-Net has 5 ResNet blocks per stage for PCA and coordinates inputs, and for the SDF input there are 3 ResNet blocks per stage. Firstly, the input data are mapped to a 64-channel feature map via a lifting convolution layer. Then the data are progressively downsampled via the encoder, which consists of a series of residual convolution blocks and max-pooling layers. For each ResNet block, the spatial resolution and number of feature channels remain unchanged, while each max-pooling layer halves the spatial resolution and doubles the feature channels.

After the bottleneck, as a symmetric architecture, the data are upsampled to gradually restore their original resolution while reducing the feature channels. For each upsampling layer, the data resolution is doubled while the feature channel halves. The upsampled features are then concatenated with the corresponding features from the encoder via skip connections, enhancing the fusion of low- and high-resolution information and helping to recover details lost during downsampling.

The condition parameters, including the sampling time step  $t$  and flow and aerodynamic labels ( $Ma$ ,  $Re$ ,  $AOA$ ,  $C_L$ ,  $C_D$ ), are added to each ResNet block in the Unet via a fully connected linear perceptron layer, ensuring that the model

is consistently constrained by the conditions. The conditions are embedded using a sinusoidal position embedding.

For PCA-based and coordinates-based diffusion, the model uses 1D convolutional layers with kernel size  $3 \times 1$ , while 2D convolutional layers with kernel size  $3 \times 3$  are used for SDF-based diffusion. Padding of size 2 is applied in all cases.

The training of all three models are carried out on an Nvidia RTX 5080, with details for each of the three data formats shown in Table 2. All models were trained using the AdanW optimizer [30] with a learning rate of 0.0001, and a cosine annealing learning rate scheduler is adopted as a standard deep learning practice. All hyper-parameters are kept identical for all three data structures.

**Table 2 Summary of Diffusion Model Training Details with the Three Data Formats**

Data Format	Model Param No.	Batch Size	Epochs	Training Time (hrs)
PCA	61,785,601	64	100	~12
Coordinates	61,785,986	64	100	~24
SDF	100,625,665	32	50	~72

## D. Model Deployment and Evaluation

### 1. Geometry Generation

The trained diffusion model can then be used to generate airfoils using Algo. 1 with specified flow conditions ( $Ma$ ,  $Re$ , and  $AOA$ ) and aerodynamic targets ( $C_L$  and  $C_D$ ). The actual  $C_L$  and  $C_D$  values of the generated profiles are validated using XFOIL, and ideally, the predicted values should match the target values.

However, the aerodynamic performance of an airfoil is highly sensitive to its geometry, such that even small geometric differences can result in significant variations in aerodynamic characteristics. The stochasticity of the diffusion sampling process also inevitably causes geometry fluctuations. Consequently, the model-generated geometries may not always achieve the desired  $C_L$  and  $C_D$  values, and multiple trials may be required to satisfy the target values within a specified tolerance  $\varepsilon$ . Therefore, the single target geometry generation workflow used in this paper is illustrated by Fig. 6a. As the tolerance  $\varepsilon$  becomes tighter, the design difficulty increases, requiring more design generation trials from the model.

### 2. Performance Evaluation

To quantify the model error, the root-mean-square error (RMSE) of the generated airfoil  $C_L$  and  $C_D$  values is also computed after the single-target generation process, as defined in Eq. (5), where  $N_{\text{test}}$  is the number of testing samples.

$$\text{RMSE}_{C_L} = \sqrt{\frac{1}{N_{\text{test}}} \sum_{i=1}^{N_{\text{test}}} \left( \frac{C_{L,i}^{\text{actual}} - C_{L,i}^{\text{target}}}{C_{L,i}^{\text{target}}} \right)^2} \quad \text{RMSE}_{C_D} = \sqrt{\frac{1}{N_{\text{test}}} \sum_{i=1}^{N_{\text{test}}} \left( \frac{C_{D,i}^{\text{actual}} - C_{D,i}^{\text{target}}}{C_{D,i}^{\text{target}}} \right)^2} \quad (5)$$

In this study, tolerances ( $\varepsilon$ ) of  $C_L$  and  $C_D$  in Fig. 6a are set to be 1 % and 5 %, respectively. A maximum of 100 design trials is allowed; if the errors are still larger than the tolerance, the best performing geometry with the lowest RMSE error is selected. The number of trials required to generate a design within the tolerance of reaching target  $C_L$  and  $C_D$  (100 if maximum design trials are reached) is recorded as a measure of effectiveness of the generative model.

In addition, it is noticed that there are also cases where the XFOIL fails to converge with the generated airfoil profile. This is usually caused by the lack of smoothness of the generated profiles, and these designs are considered as physically unfeasible. A model failure rate is hence defined as the percentage of the testing set that can not generate any feasible designs after maximum design trials as a reflection of model robustness.

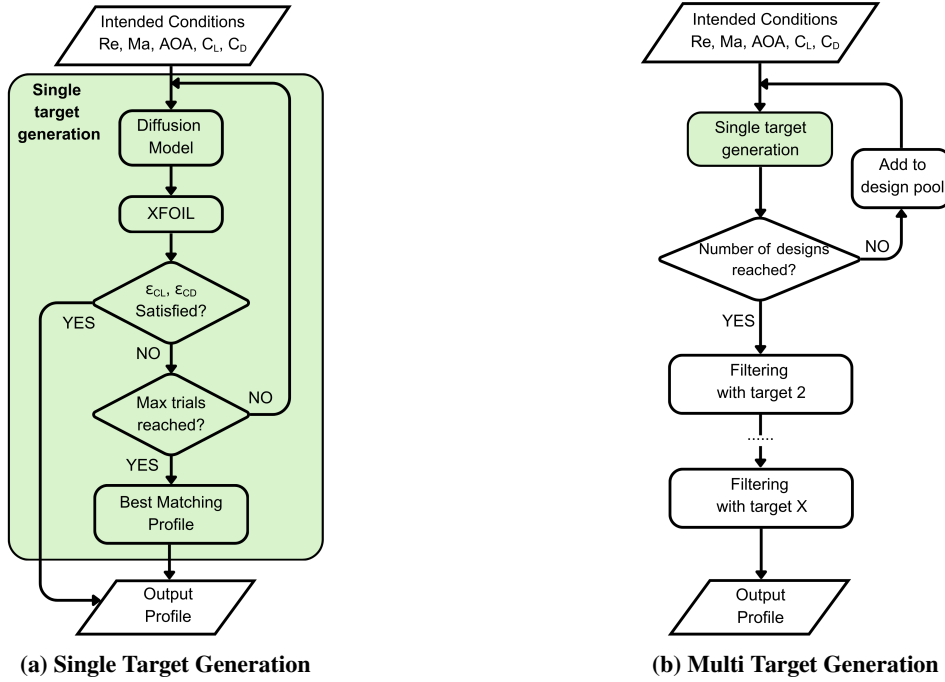


**Fig. 6 Diffusion Model Generation Procedure**

## E. Model Applications

### 1. Single-target generation

The single-target generation procedure following the work flow illustrated in Fig. 6a, with the aerodynamic target  $C_L$  and  $C_D$  being the only design objectives. In this study, the model's single-target design ability is investigated from several aspects, from interpolation to extrapolation.

**In-distribution** The model is tasked with the testing set samples, which are essentially an interpolated subset from the training set. This is the most standard way of diffusion model deployment, and is also used in this study to compare the model performances across the three different data formats.

**Continuous Condition Interpolation** To reduce data volume, the training set uses a coarse, discretised grid of flow conditions in Section. II.A.1. Since the flow conditions are physically continuous, we evaluate model’s continuous interpolation ability by introducing a test set with off-grid flow conditions (i.e. intermediate values between the training levels of  $Re$ ,  $M$ , and  $AOA$ ), and compare performance against the in-grid baseline. To achieve this, the testing set samples flow conditions are perturbed randomly such that they are at intermediate values compared to the training labels (e.g.,  $Re = 280000$ ,  $Ma = 0.15$ ,  $AOA = 2.5$ ).

**Aerodynamic Extrapolation** To test the ability of aerodynamic extrapolation ability, the model is tasked to generate airfoils with target  $C_L$  values outside the boundary of the training dataset. Training data’s Pareto front, which in this paper is defined as the best aerodynamically performing samples with the highest lift-to-drag ratio under a given flow condition, is first identified for each flow condition. An illustration of the Pareto front is shown in Fig. 7 for  $Re = 250000$ ,  $Ma = 0.2$ ,  $AOA = 3$ . The model is then used to generate airfoils that surpass the performance under the same flow condition ( $Re$ ,  $Ma$ , and  $AOA$ ) of the training set Pareto front by gradually increasing  $C_L$  with the same  $C_D$ .

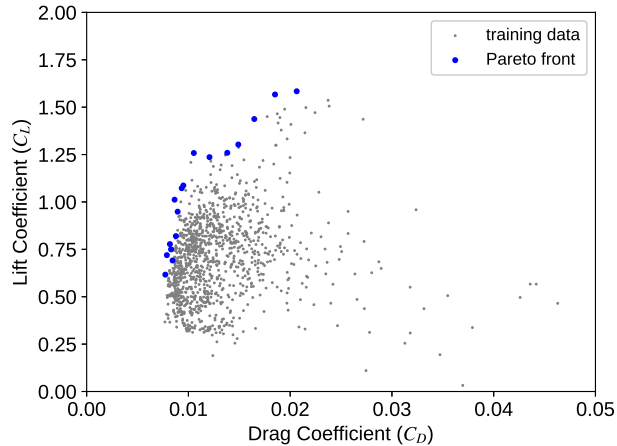


**Fig. 7 Distribution of the Testing Samples in an Example Flow Condition  $Re = 250000$ ,  $Ma = 0.2$ ,  $AOA = 3$ . The Pareto front before optimization is marked with blue points.**

**Flow Condition Extrapolation** To investigate the model’s extrapolation ability, a testing set with flow condition values sampled outside the training dataset boundary. Four featuring extrapolated flow conditions are selected for this test, as listed in Table 3.

## 2. Multi-target Design

As explained in Section I, the stochastic nature of the diffusion model is particularly advantageous for inverse design problems, as it enables the generation of diverse designs that satisfy the specified targets. This property allows

**Table 3 Extrapolated Flow Conditions**

Case	Extrapolated Quantity	Re	Ma	AOA	C <sub>L</sub>	C <sub>D</sub>
1	<i>Re</i>	400000	0.6	5	0.55	0.04
2	<i>AOA</i>	250000	0.5	-1	0.5	0.03
3	<i>Ma</i>	300000	0.7	3	0.5	0.03
4	All	400000	0.7	-1	0.4	0.03

for more effective exploration of the design space and the identification of multiple feasible solutions for a given set of conditions, making diffusion models especially suitable for multi-target design workflows. An example workflow of the multi-objective design generator is shown in Fig. 6b. By default, the first target corresponds to the target  $C_L$  and  $C_D$  at the given flow condition. Additional targets can be specified as needed, and can be geometric, (e.g. leading edge radius and maximum thickness) or off-design performance (e.g. stall limit,  $C_L$  and  $C_D$  at a different flow condition). As the number of targets or objectives increases and the tolerance for each target becomes tighter, more design trials are required to satisfy all objectives.

As shown by Fig. 6b, the single-objective generation procedure (Fig. 6a) is applied repeatedly to collect a series of designs that satisfy the  $C_L$  and  $C_D$  targets, after which the resulting design pool is filtered according to the additional objectives. While this multi-objective design workflow involves repeated sampling, it is not a purely random search of the design space. Each generated geometry is conditioned on the target  $C_L$  and  $C_D$ , leveraging the learned distribution of feasible designs. The stochastic nature of the diffusion model allows multiple distinct designs to satisfy the same aerodynamic targets, naturally capturing the one-to-many mapping of the inverse problem.

By combining repeated single-objective generation with filtering according to secondary objectives, the workflow performs an efficient, guided stochastic exploration of the design space, enabling diverse solutions that meet multiple targets simultaneously. In this study, the stall-point angle of attack ( $AOA$ ) is used as a secondary target to demonstrate the multi-target generation workflow, illustrating how diverse and feasible solutions can be efficiently explored using diffusion model.

### III. Results

#### A. Single Target Generation Results

##### 1. *In-distribution*

The sampling process of diffusion model with each data format is illustrated in Fig. 8. Four noise levels of  $\sigma = 0, 0.2, 11$ , and  $20$  are displayed to present the forward and reverse diffusion process. For the ordered coordinate- and SDF-based geometry representations, the denoising process can be directly observed in the physical design space, where initially noisy and irregular profiles (on the left in Fig. 8) are gradually denoised into smooth and physically meaningful

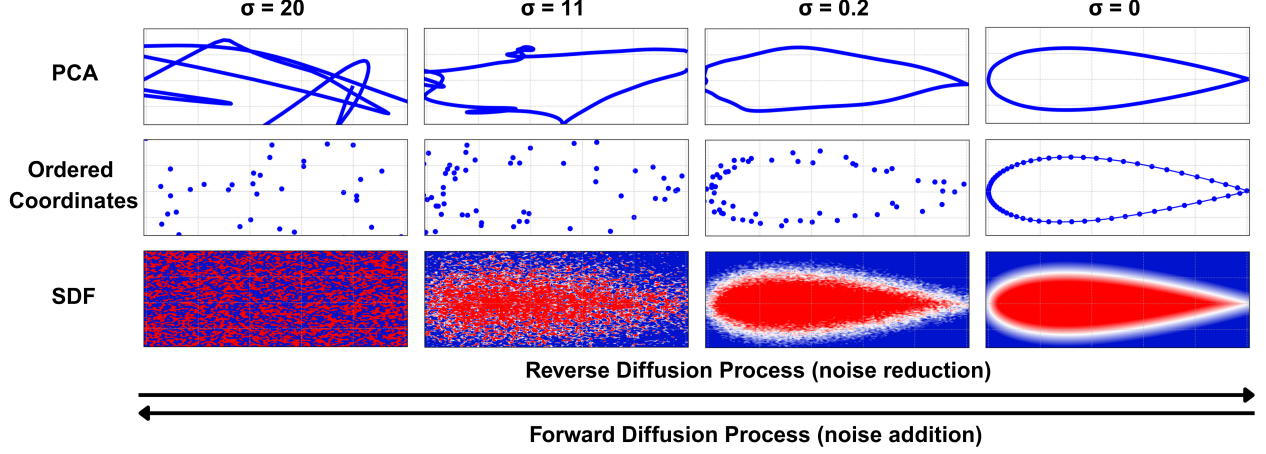


**Fig. 8 Denoising Process of three geometry encoding methods: principal component weights, ordered coordinates and signed distance function.  $\sigma$  represents the noise level**

airfoil boundaries (on the right in Fig. 8). In contrast, for the PCA-based representation, the diffusion process operates in the latent space of principal component weights as explained in Section II.A.2. As a result, the denoising behaviour is not directly visible in the geometry space in Fig. 8 for PCA-based method, and sensible airfoil shapes only emerge after the denoised principal component weights are linearly combined to reconstruct the final geometry.

Six example airfoil profiles generated using the single-target generation workflow (Fig. 6a) are shown in Fig. 9 for comparison. All generated profiles are smooth and free from geometric artifacts, indicating that the diffusion models successfully capture the underlying shape manifold of the training data for all three data structures. Despite being conditioned on identical target aerodynamic coefficients, the generated profiles exhibit noticeable geometric differences across the three data representations. This diversity arises from the stochastic nature of the diffusion sampling process and reflects the inherent one-to-many mapping of the inverse design problem. Such variability is desirable, as it provides multiple feasible design candidates that satisfy the same performance targets, offering greater flexibility for downstream design selection and optimization.

**Table 4 Single Target Generation Results**

Data Format	$C_L$ RSME	$C_D$ RSME	Average Trials	Unfeasible Designs
PCA	3.1%	8%	61	0.13 %
Coordinates	<b>0.15%</b>	<b>7.5%</b>	<b>56</b>	<b>0 %</b>
SDF	2.9%	10%	78	0.67%

To better visualise the model performance, the testing set results of single-target generation are presented in Fig. 10. The XFOIL-calculated aerodynamic metrics ( $C_L$  and  $C_D$ ) of generated airfoil profiles are plotted against the specified targets in Fig. 10. The  $C_L$  and  $C_D$  are presented on the left and right, respectively, and the zero-error line  $y = x$  is shown with red dashed lines for reference. The performance metrics are then summarized in Table 4. All three models

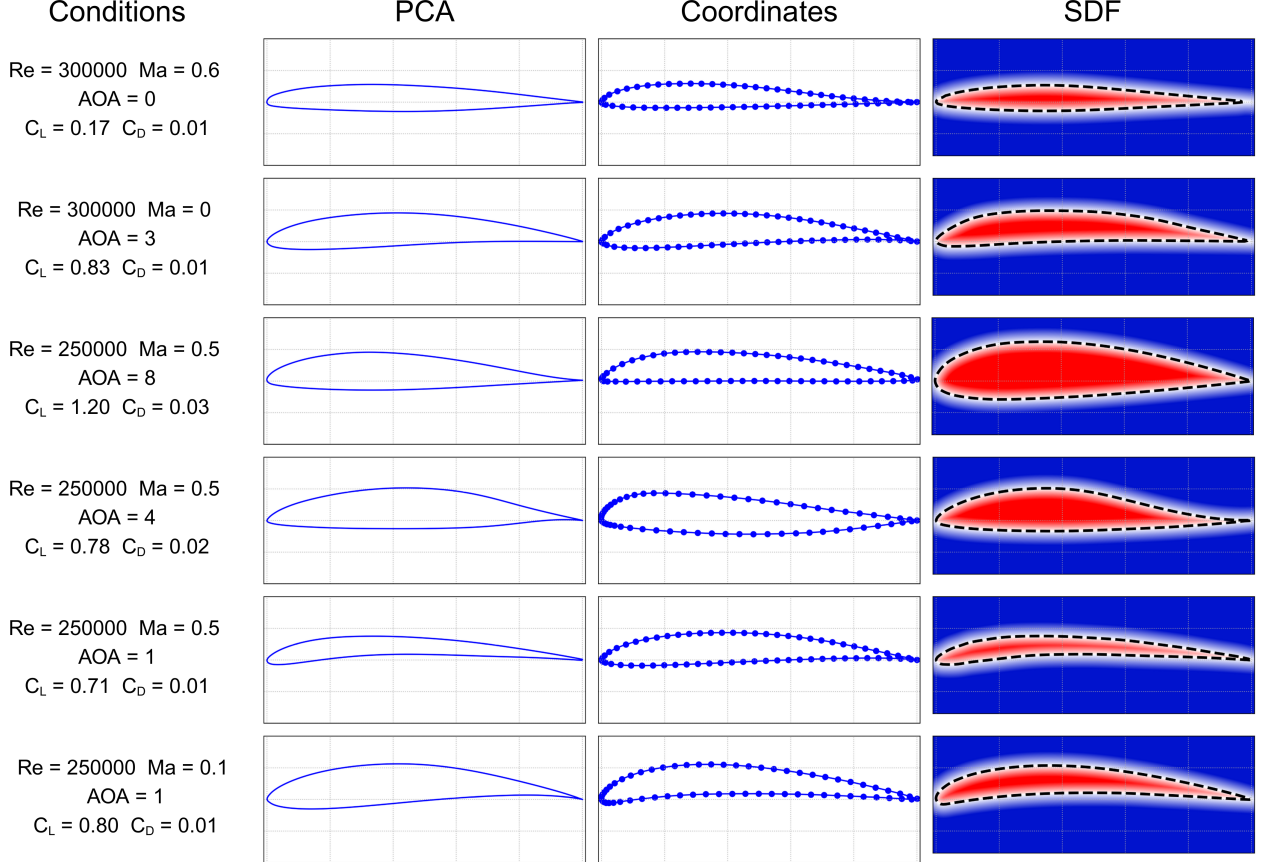


**Fig. 9 Examples of Generated Profiles**

are able to generate physically feasible airfoils within specified tolerances for the majority of the specified conditions.

It can be seen that, in the case of single target generations, the diffusion model trained with ordered coordinates performs the best across all metrics. It achieves the target  $C_L$  and  $C_D$  values with the least number of trials, results in the lowest RMSEs, and generates no unfeasible profiles as shown in Table 4. The PCA-based model performs slightly worse than the ordered coordinates model. SDF-based model exhibits the lowest performance metrics among the three data representations, yet it still achieves reasonable agreement, as shown in Fig. 10.

In terms of the model robustness of generating smooth, physically feasible airfoils, although in literature it is reported that latent space diffusion (PCA and CST) provides the advantages of smoothness guarantee compared to explicit diffusion (coordinates and mesh) [16], it is observed that PCA-based diffusion model still resulted in a small number of unfeasible designs, whereas for ordered coordinates there is no single occurrence of such case in our testing set. SDF results in the greatest amount of unfeasible designs. This is partially due to the insufficient training data explained in the previous paragraph, and may also because of the lower effective resolution of SDF compared to coordinates. The additional post-processing steps, including the quadratic interpolation and coordinates reordering, increases the chance of loss of smoothness, leading to XFOIL convergence failure and hence have the highest percentage of 0.67 %

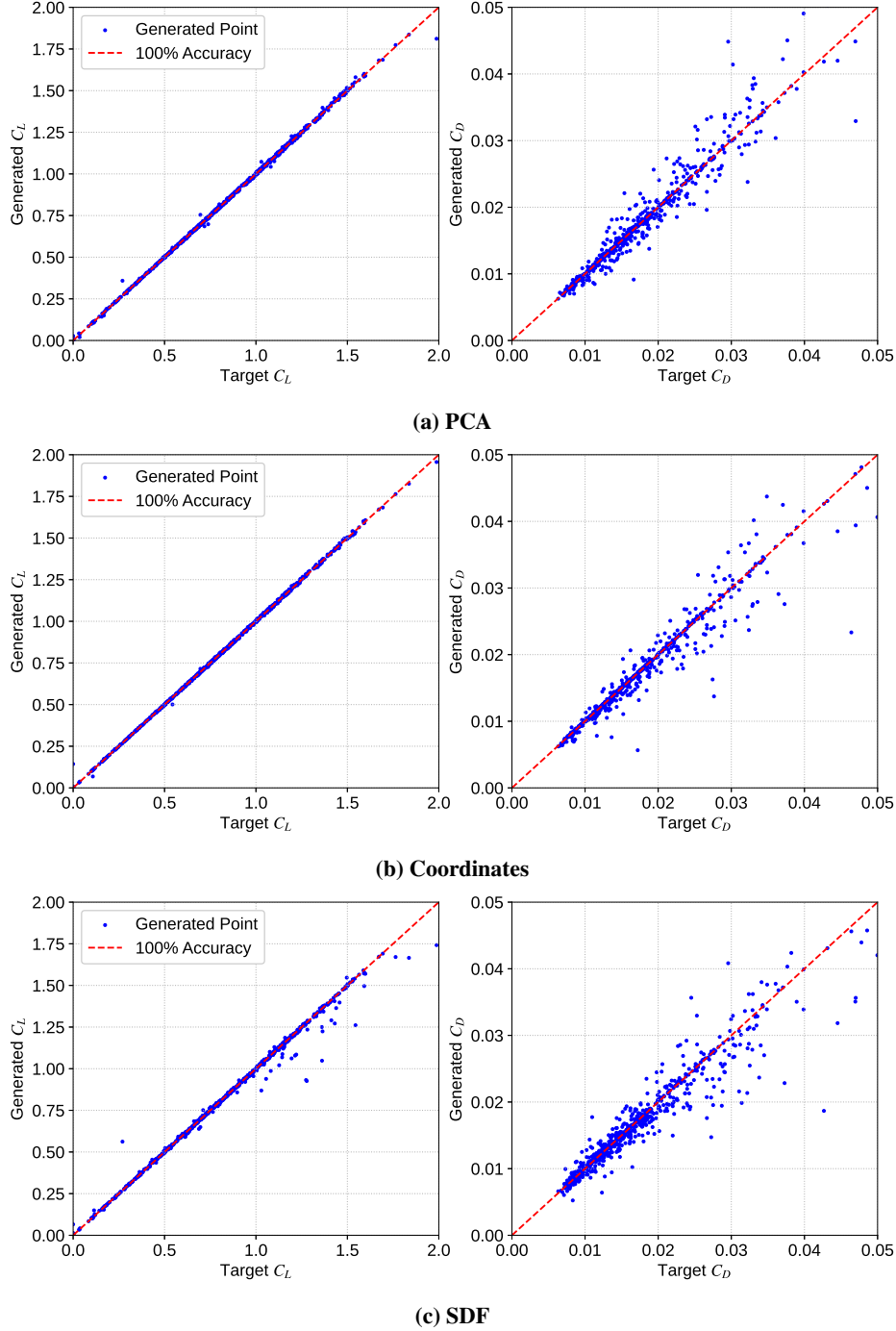


**Fig. 10 Single Target Generation Testing Set Results**

of unfeasible designs in Table 2. It is also noticed that for all three geometry encoding approaches, the error associated with  $C_D$  label is significantly larger than  $C_L$ . This is because the  $C_D$  values are at a order of magnitude smaller than  $C_L$  values, and hence it will be more sensible to geometry changes than  $C_L$ .

## 2. Continuous Condition Interpolation

The results for testing set cases with continuously interpolated flow conditions are shown in Fig. 11 and in Table. 5. The results are similar to the ones in Section III.A.1 – the ordered coordinate-based model performs the best, followed by the PCA-based model. The SDF-based model shows the worst performance among three data structures again.

Additionally, compared to the corresponding Table. 4, where all the flow conditions are the same as in the training set, the model retains the same level of performance on continuously interpolated flow conditions. This indicates that, despite the condition labels in the training set is discrete, the model still managed to capture the continuous relationship between geometry and the condition label well.

**Table 5 Single Target Generation with Continuous Condition Interpolation Results**

Data Format	$C_L$ RSME	$C_D$ RSME	Average Trials	Unfeasible Designs
PCA	<b>3.2%</b>	8%	61	0.40 %
Coordinates	3.4%	<b>7.3%</b>	<b>56</b>	<b>0.00 %</b>
SDF	4%	11%	84	0.50%

## 3. Aerodynamic Extrapolation

The aerodynamic extrapolation results using the single target generation procedure are shown in Fig. 12 and in Table 6. Similar trend can be observed here again. The coordinates-based diffusion model achieves the greatest amount of successful optimizations with the greatest  $C_L$  increments. The PCA-based diffusion model performs slightly worse. The SDF-based model completely failed in this aerodynamic extrapolation test – not only it failed to achieve a single case of successful optimization, it also could not recover the original Pareto front of the training dataset. This is likely due to the insufficient training data and low effective resolution as explained previously. The the low training data density at the Pareto front is insufficient to train the SDF-based model.

These results proves the excellent extrapolation ability of the coordinate-based diffusion model beyond the aerodynamic limits of the training set. It is also noted that the optimization at the higher  $C_D$  region is more likely to success compared to the low  $C_D$  region. This could be due to the original Pareto front at the low-drag region already reaching the aerodynamic limits. Although the diffusion model shows the ability to extrapolate aerodynamically, it cannot generate airfoils that exceeds the limits of physics, and hence is unable to optimize these points further.

**Table 6 Aerodynamic Extrapolation Results**

Data Format	No. Successful Optimization	Average $C_L$ Increment
PCA	6	3 %
Coordinates	<b>12</b>	<b>5 %</b>
SDF	0	N/A

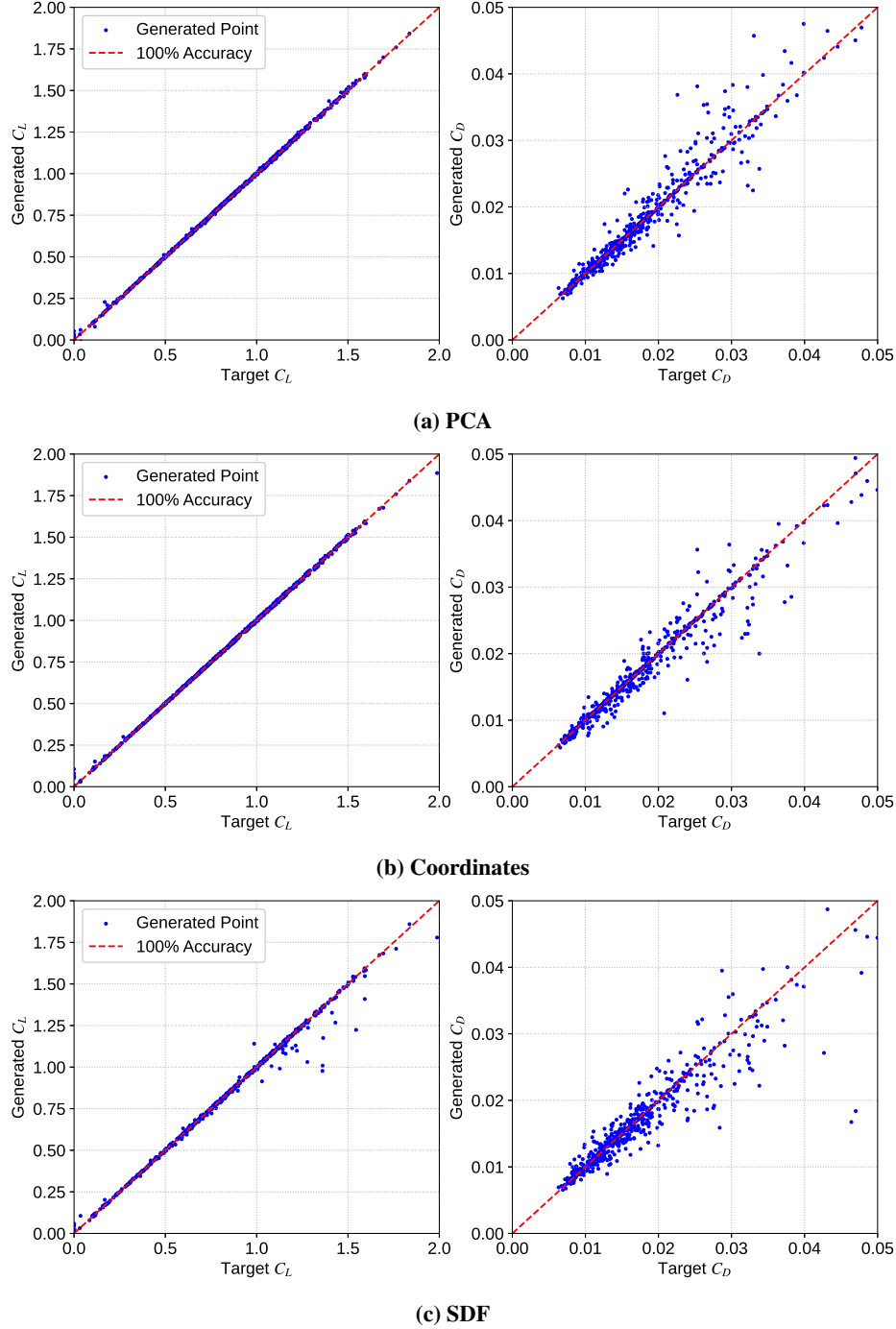


**Fig. 11 Single Target Generation with Intermediate Flow Conditions Results**

#### 4. Flow Condition Extrapolation Results

The single target generation results for the testing cases in the selected extrapolated flow condition (Table. 3) are shown in Table. 7. Overall, airfoils generated by the coordinate-based model achieves aerodynamic performance in best agreement with the targeted values, indicating the zero-shot extrapolation capability of the model.

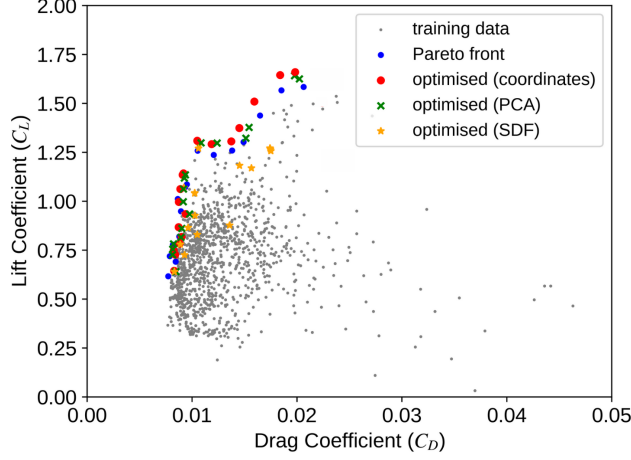


**Fig. 12 Aerodynamic Extrapolation Results**

**Table 7 Extrapolated Flow Conditions Results**

Case	PCA		Coordinates		SDF	
	$C_L$ Error	$C_D$ Error	$C_L$ Error	$C_D$ Error	$C_L$ Error	$C_D$ Error
1	<b>3.49 %</b>	9.42 %	7.61 %	<b>3.81 %</b>	6.05 %	24.6 %
2	0.98 %	4.33 %	<b>0.12 %</b>	13.4 %	3.02 %	<b>0.03 %</b>
3	1.16 %	10.2 %	<b>1.01 %</b>	<b>0.62 %</b>	1.23 %	11.7 %
4	0.68 %	<b>3.33 %</b>	<b>0.20 %</b>	13.8 %	5.42 %	4.77 %

### 5. Discussion

Overall, there is a clear trend that the diffusion model trained with ordered coordinates outperforms the other two models (PCA- and SDF-based models), showing superior performance across all performance evaluations, including aerodynamic performance error, average number of trials, unfeasible designs, interpolation, and extrapolation. The underlying reason that affects the model performance is the geometric information encoding process.

For the ordered coordinates-based model, the geometric information is directly encoded and learned by the 1D convolutional neural layers of the diffusion model. The ordered arrangement of coordinates, as illustrated in Fig. 3, preserves spatial continuity along the airfoil surface, enabling the convolution layers to efficiently extract the geometric features of the airfoil profiles.

In contrast, for the PCA-based diffusion, the geometric information is represented implicitly in latent space through the PCA transformation. The input of the diffusion model consists of a set of principal components weights, which do not retain explicit spatial information. As a result, the convolutional layers are less effective at exploiting their inherent advantage in local geometric feature extraction, making it more challenging for the model to learn the mapping from the condition labels to the corresponding airfoil geometries. In addition, as discussed in Section I, latent-space diffusion inherently reduces the effective design space through dimensionality compression. While this can improve training efficiency, it may also limit the diversity of generated solutions. For inverse design problems, which are intrinsically

one-to-many, this reduction in design space can be unfavorable when a wide variety of feasible designs is desired.

Among the three data representations, the 2D SDF-based diffusion model exhibits the lowest performance. This is primarily attributed to the increase in data dimensionality from 1D to 2D, which substantially raises the amount of trainable parameters, as shown in Table 2, and consequently increases the amount of training data required. Therefore, for the same training dataset size, the SDF-based model underperforms compared to 1D geometry encodings like PCA and coordinates. In addition, the SDF representation relies on a discretized grid with finite resolution, which introduces a trade-off between geometric fidelity and computational cost. Limited resolution can lead to loss of fine geometric details and increased numerical diffusion during the denoising process.

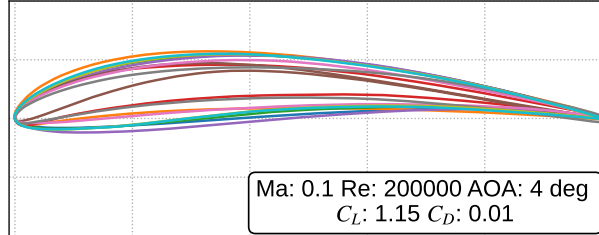
Nevertheless, the promising results presented demonstrate the feasibility of using SDF to encode airfoil geometries for diffusion-based aerodynamic shape generation. As an implicit and continuous representation of geometry, the SDFs are well suited for representing high-dimensional geometric data in a continuous space, especially when the object can be described implicitly by a boundary, making it particularly suitable for complex geometric learning tasks such as 3D shape generation in engineering. The SDF work presented in this paper hence provides a clear pathway towards 3D shape generation, where higher-dimensional SDFs are particularly advantageous [19].

## B. Multi Targets Generation

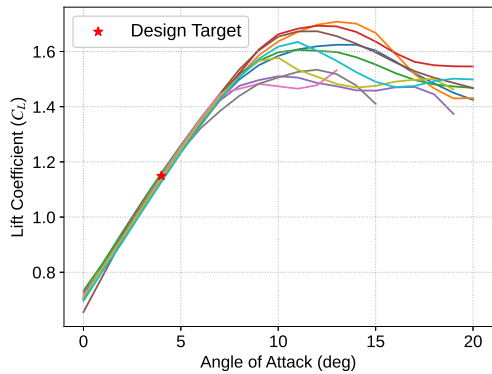
As discussed in Section II.D, the stochasticity of the diffusion model aligns with the nature of inverse design problems, which by definition is a one-to-many mapping. Therefore, there will be more than one possible geometries present which share the same  $C_L$  and  $C_D$  values under the same flow conditions. Figure 13a shows an example of this non-deterministic mapping. To demonstrate the multi-targets generation workflow in Fig. 6b, ten different geometries are generated and all of them satisfy the  $C_L$  and  $C_D$  targets under the specified flow condition (labeled on the bottom right of Fig. 13a). By doing so, a design pool of 10 airfoils that all satisfy the aerodynamic design target ( $C_L$  and  $C_D$ ) is formed. These designs can be further selected with different targets. The coordinate-based diffusion model, which shows the best performance in the single-target generation tasks, is used in this demonstration.

As an example of the multi-target generation, the off-design aerodynamic performance is evaluated by computing the  $C_L$  and  $C_D$  curves under the design flow conditions ( $Ma$  and  $Re$ ) but at off-design angles of attacks ( $AOA$ ), as shown in Figs. 13b and 13c. The ten designs exhibit significantly different off-design performances, and the best performing profile can be selected according to the particular application requirement. For instance, if one requires the profile to have highest possible stall  $AOA$ , the orange profile will be selected. In fact, this selection can be applied to any targets, both geometrically and aerodynamically.

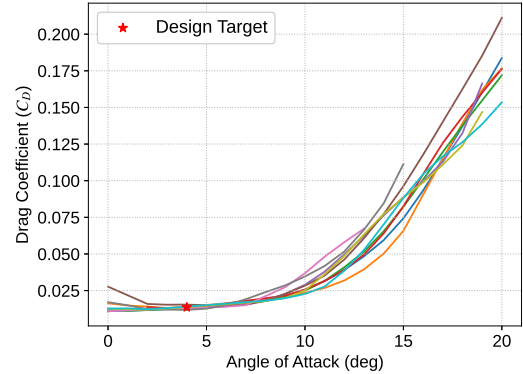
Compared to the diffusion-model based multi-target generation approaches proposed in the literature, the presented method shows greater flexibility in real engineering applications. The multi-target generation paradigm proposed in the literature is to encode all the design targets as the condition label of the model [11, 13], which may include maximum



(a) Feasible Design Pool



(b)  $C_L$  at Off-design AOAs



(c)  $C_D$  at Off-design AOAs

Fig. 13 Multi Targets Generation Results

thickness, off-design performance, leading edge radius and so on. The generation process will therefore inherently become a one-shot multi-target generation process as shown in Fig. 6a. While providing more controllability of the secondary design targets, this approach also reveals several drawbacks. The most obvious one is the need of preparing additional condition labels, which may include geometric labels and off-design performances. The additional conditions also increases the scale of the neural network needed and hence the training complexity. More importantly, the diffusion model trained with this approach will be case-specific and not universally applicable. If one wants to change the design targets (e.g., additional design requirements), the diffusion model will need to be re-trained with the new sets of design targets as the condition label. In contrast, despite our proposed method requires multiple design trials and post-filtering, it is also more flexible.

#### IV. Conclusion

In summary, a diffusion-based inverse-design framework for airfoils is introduced in this study, with  $Re$ ,  $Ma$  and  $AOA$  as the flow conditions, and with  $C_L$  and  $C_D$  as the aerodynamic design targets. The model achieved accurate, constraint-satisfying generation across broad ranges of flow conditions, which sets the new state-of-the-art against the previous works in the literature. The conclusions and major contributions of this study are as follows.

- 1) Diffusion model is implemented as a novel paradigm of airfoil generation. By adopting the state-of-the-art EDM diffusion sampling method, jointly with multi-flow condition labeling of  $Ma$ ,  $Re$ , and  $AOA$  across broad

ranges, we delivered an effective, unified diffusion model workflow to generate airfoil geometries that satisfy to the given design targets accurately.

- 2) We provide the first systematic comparison of using different airfoil shape encoding data formats to train the diffusion model. Using the same diffusion backbone and the same U-Net architecture with ResNet blocks, three different encoding methods are implemented and compared: PCA-based method using PC weights, ordered x-y coordinate, and SDF-based method using discretized 2D SDF values. The training effectiveness is evaluated from a wide range of perspectives, including both interpolation and extrapolation of the training dataset. The model's ability to generalize to interpolate at continuous flow condition labels is also tested by providing inputs that lie between the discrete values in the training set. The extrapolation ability is examined both aerodynamically, by tasking the diffusion model with  $C_L$  target beyond the Pareto front of the training dataset, as well as with respect to flow conditions by tasking the model with flow conditions beyond the range of the training set.
- 3) The comparison results consistently indicate that the model trained with coordinates outperform the PCA format on aerodynamic targets due to the explicit spatial encoding in its data structure, both with interpolation and extrapolation test sets. In addition, despite SDF training data resulted in less performing model, it proves its feasibility in the field of aerodynamic shape generation, paving the way towards 3D shapes where SDF with more natural spatial encoding and scalability.
- 4) Based on the stochastic nature of the design generation with diffusion model, we introduced multi-target design generation workflow using the trained diffusion model in engineering optimizations. In this paper the diffusion model is deployed multiple times to collect a pool of designs that all satisfies the aerodynamic design target, from where the designs can be further filtered according to the particular application requirements.

## References

- [1] Jacobs, E. N., Ward, K. E., and Pinkerton, R. M., “The characteristics of 78 related airfoil sections from tests in the variable-density wind tunnel,” Tech. rep., NASA, 1933.
- [2] Martins, J. R. R. A., “Aerodynamic Design Optimization: Challenges and Perspectives,” *Computers & Fluids*, Vol. 239, 2022, p. 105391. <https://doi.org/10.1016/j.compfluid.2022.105391>.
- [3] Samareh, J., “Aerodynamic Shape Optimization Based on Free-Form Deformation,” *10th AIAA/ISSMO Multidisciplinary Analysis and Optimization Conference*, American Institute of Aeronautics and Astronautics, Albany, New York, 2004, pp. 1–12. <https://doi.org/10.2514/6.2004-4630>.
- [4] Sharpe, P., and Hansman, R. J., “NeuralFoil: An Airfoil Aerodynamics Analysis Tool Using Physics-Informed Machine Learning,” , Mar. 2025. <https://doi.org/10.48550/arXiv.2503.16323>.

[5] Drela, M., “XFOIL: An Analysis and Design System for Low Reynolds Number Airfoils,” *Low Reynolds Number Aerodynamics*, edited by T. J. Mueller, Springer, Berlin, Heidelberg, 1989, pp. 1–12. [https://doi.org/10.1007/978-3-642-84010-4\\_1](https://doi.org/10.1007/978-3-642-84010-4_1).

[6] Wang, J., Li, R., He, C., Chen, H., Cheng, R., Zhai, C., and Zhang, M., “An Inverse Design Method for Supercritical Airfoil Based on Conditional Generative Models,” *Chinese Journal of Aeronautics*, Vol. 35, No. 3, 2022, pp. 62–74. <https://doi.org/10.1016/j.cja.2021.03.006>.

[7] Tan, X., Manna, D., Chattoraj, J., Yong, L., Xinxing, X., Ha, D. M., and Feng, Y., “Airfoil Inverse Design Using Conditional Generative Adversarial Networks,” *2022 17th International Conference on Control, Automation, Robotics and Vision (ICARCV)*, 2022, pp. 143–148. <https://doi.org/10.1109/ICARCV57592.2022.10004343>.

[8] Lei, R., Bai, J., Wang, H., Zhou, B., and Zhang, M., “Deep Learning Based Multistage Method for Inverse Design of Supercritical Airfoil,” *Aerospace Science and Technology*, Vol. 119, 2021, p. 107101. <https://doi.org/10.1016/j.ast.2021.107101>.

[9] Ho, J., Jain, A., and Abbeel, P., “Denoising Diffusion Probabilistic Models,” , Dec. 2020. <https://doi.org/10.48550/arXiv.2006.11239>.

[10] Dhariwal, P., and Nichol, A., “Diffusion Models Beat GANs on Image Synthesis,” , Jun. 2021. <https://doi.org/10.48550/arXiv.2105.05233>.

[11] Diniz, C., and Fuge, M., “Optimizing Diffusion to Diffuse Optimal Designs,” *AIAA SCITECH 2024 Forum*, American Institute of Aeronautics and Astronautics, Orlando, FL, 2024, pp. 1–22. <https://doi.org/10.2514/6.2024-2013>.

[12] Wei, Z., Dufour, E. R., Pelletier, C., Fua, P., and Bauerheim, M., “DiffAirfoil: An Efficient Novel Airfoil Sampler Based on Latent Space Diffusion Model for Aerodynamic Shape Optimization,” *AIAA AVIATION FORUM AND ASCEND 2024*, American Institute of Aeronautics and Astronautics, 2024, pp. 1–18. <https://doi.org/10.2514/6.2024-3755>.

[13] Wen, Z., Lian, Y., Zeng, L., Tian, C., Li, J., and Shao, X., “Airfoil-DDPM: A Flexible Airfoil Generative Design Method Using a Multi-Objective Sampling Based Diffusion Model,” *Aerospace Science and Technology*, Vol. 168, 2026, p. 111070. <https://doi.org/10.1016/j.ast.2025.111070>.

[14] Zhuang, Y., Hedayat, A., and Jacobsen, C., “A Surrogate-based Optimisationn Framework Augmented by Generative AI,” , 2025. <https://doi.org/https://github.com/tonyzyl/Diffusion-based-2DAirfoil-Generation>.

[15] Deng, S., Zhang, Q., and Cai, Z., “Generative Method for Aerodynamic Optimization Based on Classifier-Free Guided Denoising Diffusion Probabilistic Model,” *Structural and Multidisciplinary Optimization*, Vol. 68, No. 8, 2025, p. 165. <https://doi.org/10.1007/s00158-025-04111-x>.

[16] Wagenaar, T., Mancini, S., and Mateo-Gabín, A., “Generative Aerodynamic Design with Diffusion Probabilistic Models,” , Sep. 2024. <https://doi.org/10.48550/arXiv.2409.13328>.

[17] Luo, S., and Hu, W., “Diffusion Probabilistic Models for 3D Point Cloud Generation,” *2021 IEEE/CVF Conference on Computer Vision and Pattern Recognition (CVPR)*, 2021, pp. 2836–2844. <https://doi.org/10.1109/CVPR46437.2021.00286>.

[18] Smith, E., and Meger, D., “Improved Adversarial Systems for 3D Object Generation and Reconstruction,” , Nov. 2017. <https://doi.org/10.48550/arXiv.1707.09557>.

[19] Park, J., Lee, Y., and Kim, J., “Multi-Modal Conditional Diffusion Model Using Signed Distance Functions for Metal-Organic Frameworks Generation,” *Nature Communications*, Vol. 16, No. 1, 2025, p. 34. <https://doi.org/10.1038/s41467-024-55390-9>.

[20] Graves, R., and Farimani, A. B., “Airfoil Diffusion: Denoising Diffusion Model For Conditional Airfoil Generation,” , Dec. 2024. <https://doi.org/10.48550/arXiv.2408.15898>.

[21] Karras, T., Aittala, M., Aila, T., and Laine, S., “Elucidating the Design Space of Diffusion-Based Generative Models,” , Oct. 2022. <https://doi.org/10.48550/arXiv.2206.00364>.

[22] Lin, J.-h., Chen, S.-s., Jin, S.-y., Jiang, Q.-f., Jia, M.-l., and Li, D., “Multi-Point Aerodynamic Inverse Design of Flying Wing Using the Conditional Diffusion Model,” *Physics of Fluids*, Vol. 37, No. 7, 2025. <https://doi.org/10.1063/5.0271723>.

[23] Gong, Z., and Zhao, H., “Latent Diffusion Model for Multidisciplinary and Multi-Objective Airfoil Inverse Design,” , Aug. 2024. <https://doi.org/10.36227/techrxiv.172468827.77833794/v1>.

[24] Selig, M., “UIUC Airfoil Data Site,” [https://m-selig.ae.illinois.edu/ads/coord\\_database.html](https://m-selig.ae.illinois.edu/ads/coord_database.html), 1996.

[25] Shlens, J., “A Tutorial on Principal Component Analysis,” , Apr. 2014. <https://doi.org/10.48550/arXiv.1404.1100>.

[26] Song, Y., Sohl-Dickstein, J., Kingma, D. P., Kumar, A., Ermon, S., and Poole, B., “Score-Based Generative Modeling through Stochastic Differential Equations,” , Feb. 2021. <https://doi.org/10.48550/arXiv.2011.13456>.

[27] Ronneberger, O., Fischer, P., and Brox, T., “U-Net: Convolutional Networks for Biomedical Image Segmentation,” , May 2015. <https://doi.org/10.48550/arXiv.1505.04597>.

[28] Liu, Z., Feng, Y., Black, M. J., Nowrouzezahrai, D., Paull, L., and Liu, W., “MeshDiffusion: Score-based Generative 3D Mesh Modeling,” , Apr. 2023. <https://doi.org/10.48550/arXiv.2303.08133>.

[29] He, K., Zhang, X., Ren, S., and Sun, J., “Deep Residual Learning for Image Recognition,” , Dec. 2015. <https://doi.org/10.48550/arXiv.1512.03385>.

[30] Loshchilov, I., and Hutter, F., “Decoupled Weight Decay Regularization,” , Jan. 2019. <https://doi.org/10.48550/arXiv.1711.05101>.